ACS APPLIED MATERIALS & INTERFACES

Research Article

www.acsami.org

A Highly Efficient $TiO_{2-x}C_x$ Nano-heterojunction Photocatalyst for Visible Light Induced Antibacterial Applications

Vinodkumar Etacheri,[†,‡] Georg Michlits,[‡] Michael K. Seery,[‡] Steven J. Hinder,[§] and Suresh C. Pillai*[,†]

[†]Centre for Research in Engineering Surface Technology (CREST), FOCAS Institute, Dublin Institute of Technology, Kevin Street, Dublin 8, Ireland

[‡]School of Chemical and Pharmaceutical Sciences, Dublin Institute of Technology, Kevin Street, Dublin 8, Ireland

[§]The Surface Analysis Laboratory, Faculty of Engineering and Physical Sciences, University of Surrey, Guildford, Surrey, GU2 7XH, United Kingdom

Supporting Information

ABSTRACT: Visible-light-induced antibacterial activity of carbon-doped anatase-brookite titania nano-heterojunction photocatalysts are reported for the first time. These heterostructures were prepared using a novel low temperature (100 °C) nonhydrothermal low power microwave (300 W) assisted method. Formation of interband C 2p states was found to be responsible for the band gap narrowing of the carbon doped heterojunctions. The most active photocatalyst obtained after 60 min of microwave irradiation exhibits a 2-fold higher visible-light induced photocatalytic activity in contrast to the standard commercial photocatalyst Evonik-Degussa P-25. *Staphylococcus aureus* inactivation rate constant for carbon-doped nano-heterojunctions and the standard photocatalyst was 0.0023 and −0.0081 min^{-1}, respectively. It is proposed that the photoexcited electrons (from the C 2p level) are effectively transferred from the conduction band of brookite to that of anatase causing efficient electron−hole separation, which is found to be responsible for the superior visible-light induced photocatalytic and antibacterial activities of carbon-doped anatase-brookite nano-heterojunctions.

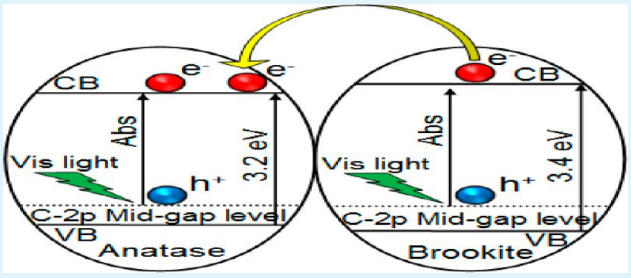

KEYWORDS: *titanium dioxide, microwave synthesis, carbon-doping, visible-light induced photocatalysis, antibacterial activity, heterojunctions*

1. INTRODUCTION

Hospital-acquired infections due to the spread of multidrug resistant bacteria, such as Methicillin-resistant *Staphylococcus aureus* (MRSA) and *Clostridium difficile* (*C.diff*) are a worldwide problem.[1] In addition to this, the occurrence of severe acute respiratory syndrome (SARS) and avian influenza (H1N5) in recent years have affected public health worldwide. Since these superbugs are resistant to most of the antibiotics available, it is necessary to develop efficient and eco-friendly antimicrobial techniques. Semiconductor photocatalysis is an efficient and inexpensive technique to solve hospital acquired infections.[2] In recent years nanostructured semiconductors, especially titanium dioxide, have attracted significant interest in the area of photocatalysis, organic synthesis, solar cells, electronic materials, cancer therapy, water and air purification, and self-cleaning antibacterial materials.[2−5] This was mainly due to the high redox potential, nontoxicity, chemical stability, and inexpensiveness of titanium dioxide photocatalysts.[3,4] Among the three polymorphs of titanium dioxide, anatase is previously reported as the most photocatalytically active phase due to its higher charge carrier mobility and increased surface hydroxyl density.[3,5] Various factors such as phase purity, surface area, crystallite size, quantity, and nature of dopants and method of preparation significantly affect the performance of titania photocatalysts.[2,4,5]

The major disadvantage of anatase phase photocatalyst is its wide band gap (3.2 eV), which make it a good photocatalyst only under UV-light ($\lambda \leq 387.5$ nm).[5] This makes the titania based photocatalysis a nonviable method for real-world antibacterial applications under visible-light or normal room-light irradiation. The development of a highly visible-light active titania photocatalyst is necessary to effectively exploit visible-light for antibacterial applications. There are a number of reports on the synthesis of graphene incorporated titania nanomaterials.[6−9] These photocatalysts containing Ti−C and Ti−O−C bonds were harmful to bacteria and minuscule animals under solar-light irradiation.[6,7] Recently, nonmetal (e.g., C, N, S, F, and B) doped titania has received much attention as the incorporation of these nonmetals into titania result in the extension of photoresponse from UV to visible regions.[10−12] One of the major disadvantage of these anion-doped titania photocatalysts is the increased electron−hole

Received: November 12, 2012
Accepted: February 5, 2013
Published: February 5, 2013

recombination due to the additional energy levels and oxygen vacancies formed in the band gap.[3,5] As a result, the photocatalytic and antibacterial activities of anion-doped anatase titania photocatalysts were not sufficient enough for practical applications. One way to overcome this problem is the proper designing of heterojunctions containing anion-doped titania and electron−hole separating agents such as metal or semiconductor nanoparticles. Significantly higher UV-light induced photocatalytic activities of anatase-rutile and anatase-brookite heterojunctions in contrast to pure anatase, rutile, or brookite alone were reported previously.[13−15] As part of a study to investigate the effect of anion doped heterojunctions, our group has recently reported superior visible-light induced photocatalytic activities of N-doped and S,N-codoped anatase-rutile nano-heterojunctions.[3,5] From these observations, it was evident that the synthesis of anion-doped titania nano-heterojunctions is necessary to obtain a significantly higher visible-light induced antibacterial activity.

Synthesis of nanocrystalline titania possessing very high surface area is a major challenge in the area of semiconductor photocatalysis. Conventionally, photocatalysts are produced by the heat treatment of amorphous titania precursor.[4,16] However, high temperature treatment for attaining crystallinity often leads to particle agglomeration, poor surface area, extreme particle growth, sintering associated with the collapse of mesoporous structure, and undesired phase formation.[3,16] These result in an apparent decrease in the photocatalytic and antibacterial activity. In comparison to a variety of chemical synthesis methods, microwave assisted hydrothermal synthesis is a suitable low temperature process to prepare high surface area submicrometer and nanosized semiconductors.[17−19] The main drawbacks of microwave and conventional hydrothermal methods are the use of organic solvents and the risk of handling pressurized containers. Therefore, these methods for the synthesis of nanosized titania photocatalysts are not environmental friendly and industrially viable. These factors demonstrate that the development of an aqueous nonhydrothermal (without using pressurized containers) microwave method is necessary for the synthesis of titania nanomaterials. To the best of our knowledge, there are no systematic studies reported for the nonhydrothermal microwave synthesis of anion-doped titania nano-heterojunctions. For the first time, carbon-doped anatase-brookite heterojunction nanoparticles possessing very high surface area, visible-light induced photocatalytic, and antibacterial activity were synthesized through an aqueous nonhydrothermal microwave method. Formation mechanism, electronic structure, physical properties, and visible-light induced photocatalytic and antibacterial activities of these nanostructured carbon-doped heterojunctions were explored.

2. EXPERIMENTAL METHODS

2.1. Microwave Synthesis of Carbon-Doped Heterojunctions. Carbon-doped anatase-brookite nano-heterojunctions were synthesized through a low temperature (100 °C) nonhydrothermal microwave method. All chemicals were purchased from Sigma Aldrich and used without further purification. In a typical synthesis, titanium tetraisopropoxide (7.5 mL) was added dropwise to an excess of deionized water (75 mL) with continuous stirring to form hydrated titanium dioxide. The suspension thus obtained was then stirred for 30 min and irradiated with microwave radiations of power 300 W in a microwave oven (CEM-MARS) for various time intervals (10, 20, 40, and 60 min). The aqueous TiO_2 suspension was again stirred for 5 min after each 10 min of microwave treatment. The microwave treated titania samples were then washed with deionized water and dried in an oven at 80 °C for 12 h and powdered well using agate mortar and pestle. No external carbon sources were used for the synthesis of visible-light active anatase-brookite nano-heterojunctions. Carbon present in the heterojunctions was self-doped by the decomposition of isopropyl alcohol (formed by the hydrolysis of titanium tetraisopropoxide) up on microwave treatment.

2.2. Characterization Techniques. A Siemens D 500 X-ray diffractometer working with Cu Kα radiation (λ = 0.15418 nm) was used for the phase analysis of anatase-brookite heterojunctions. The amounts of anatase and brookite present in the heterojunctions were calculated using eqs 1 and 2, respectively.

$$W_A = \frac{K_A A_A}{K_A A_A + K_B A_B} \quad (1)$$

$$W_B = \frac{K_B A_B}{K_A A_A + K_B A_B} \quad (2)$$

W_A and W_B represent the weight fractions of anatase and brookite respectively. A_A and A_B refer to the integrated intensity of anatase (101) and brookite (121) peaks. K_A and K_B are constants of 0.886 and 2.721, respectively. The Scherrer equation (eq 3) was used for the precise determination of anatase and rutile crystallite sizes in calcined titania samples.

$$\Phi = \frac{K\lambda}{\beta \cos\theta} \quad (3)$$

Where Φ is the crystallite size, λ is the wavelength of X-ray used; K is the shape factor, β is the full line width at the half-maximum height of the main intensity peak, and θ is the Bragg angle. Raman spectra of heterojunctions were recorded with a Dilor ISA Labram 1 B micro-Raman system equipped with a 514 nm Ar^+ ion laser. Differential scanning calorimetry (DSC) measurements were performed using a Rheometric Scientific DSC QC instrument. A Perkin-Elmer GX FTIR spectrometer was used for recording the FTIR spectra (4000−400 cm^{-1}) of titania heterojunctions. A JEOL transmission electron microscope (JEM-2100 operating at an accelerating voltage of 200 kV) was employed for the analysis of particle-loaded Formvar-coated copper grids.

The nitrogen adsorption and desorption isotherms were collected using a Quantachrome 2000e surface area analyzer. The linear portion (P/P_o = 0.05−0.2) of the Brunauer−Emmett−Teller (BET) model was used for the calculation of specific surface area. Pore diameter and volumes were calculated from the desorption branch of the Barret−Joyner−Halenda (BJH) model. A Thermo Fisher Scientific (East Grinstead, UK) Theta Probe spectrometer using monochromatic Al−Kα radiation (photon energy 1486.6 eV) was used for the X-ray photoelectron spectroscopic (XPS) studies. Charge compensation was achieved using a low-energy electron flood gun. The binding energies of all of the elements present were determined by setting the CC/CH component of the C 1s peak at 284.5 eV. Quantitative surface chemical analysis was performed using high-resolution core level spectra after the removal of a nonlinear Shirley background. Overlapping signals were analyzed after deconvolution into 30% Gaussian/70% Lorenzian shaped components. Band gap values were calculated using a Perkin-Elmer Lambda 900 UV/vis/NIR spectrometer equipped with an integrated sphere attachment using $BaSO_4$ as the reference. The Kubelka−Munk function $F(R_\infty)$ (which is equivalent to absorbance) was plotted against wavelength, and band gap values were calculated by extrapolating the lower wavelength cutoff region. Room temperature photoluminescence spectra of samples were recorded using a Perkin-Elmer Luminescence Spectrometer (LS-55B) at an excitation wavelength of 260 nm. Powder samples were dispersed in deionized water (0.01 g in 100 mL) and sonicated for 30 min prior to the analysis.

2.3. Visible-Light Induced Photocatalytic and Antibacterial Activity Evaluation. Methylene blue degradation technique was employed for investigating the visible-light induced photocatalytic activity of carbon-doped anatase-brookite heterojunctions.[3−5] A Q-Sun solar simulator and a primary blue filter with a transmission intensity

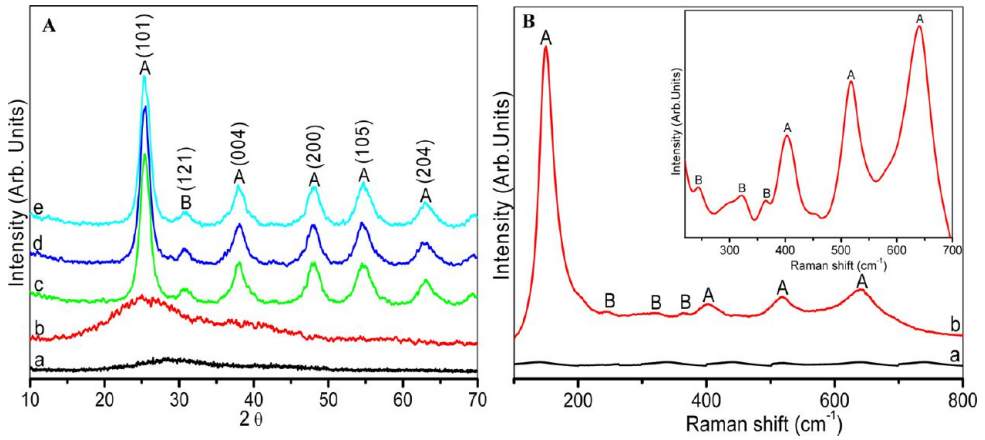

Figure 1. (A) XRD patterns of carbon-doped anatase-brookite heterojunctions prepared by microwave irradiation (a) before irradiation, (b) after 10 min, (c) after 20 min, (d) after 40 min, and (e) after 60 min irradiation. (B) Raman spectra of carbon-doped anatase-brookite heterojunctions prepared by microwave irradiation for 20 min. (A = anatase, B = brookite).

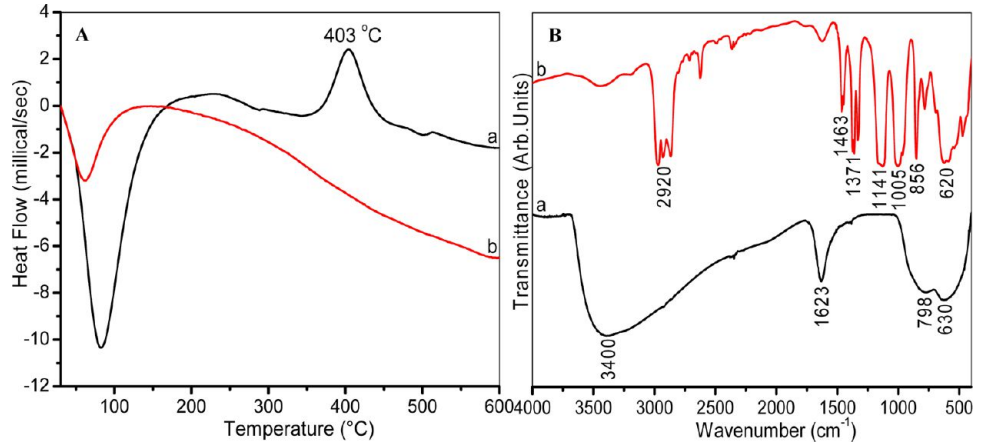

Figure 2. (A) Differential scanning calorimetric pattern of (a) amorphous TiO_2 (b) carbon-doped anatase-brookite heterojunctions prepared by 20 min microwave irradiation. (B) FTIR spectrum of (a) carbon-doped anatase-brookite heterojunctions prepared by 20 min microwave irradiation (b) titanium tetraisopropoxide.

of 45% at 450 nm (Supporting Information Figure S1) were used for the generation of polychromatic visible-light. The filter opaque to 530−680 nm light was intentionally selected to avoid the photosensitized and photolytic decomposition of methylene blue. In a typical photocatalytic degradation experiment, 50 mL of an aqueous solution of 10^{-5} M methylene blue was stirred well with 0.06 g of titania powder in a 100 mL glass beaker. The suspension thus obtained was kept under the dark for 30 min and then irradiated with visible-light (0.68 W/m^2) with stirring. An air cooler and thermostat were connected to the solar simulator to maintain the temperature of suspension at 25 °C. Aliquots (3 mL) were withdrawn from the suspension under visible-light irradiation at equal time intervals of 1 h, and the absorption spectra were recorded using a Perkin-Elmer Lambda 900 UV/vis/NIR spectrometer. The photocatalytic rate constant (k) for methylene blue degradation was determined from the first-order plot using eq 4.

$$\ln\left(\frac{A_0}{A}\right) = kt \tag{4}$$

Where, k is the first-order rate constant, A_0 is the initial absorbance, and A is the absorbance after a time t. Photocatalytic degradation experiments were repeated three times, and the calculated rate constants were within 5% error limit. A control photocatalytic experiment was also performed without using TiO_2, which confirmed almost no decomposition of methylene blue (Supporting Information Figure S2).

In order to evaluate the visible-light induced antibacterial activity, titania powder (0.01 g) was stirred with 5 mL of sterile maximum recovery diluent (MRD) for 15 min. The resulting suspension was then inoculated with 500 μL of overnight grown *Staphylococcus aureus* ATCC 25923 bacterial culture (10^5 CFU/mL). These inoculated test suspensions were then irradiated with polychromatic visible-light (0.68 W/m^2) generated by Q-Sun solar simulator and primary blue filter (450 nm). Aliquots (100 μL) of test suspension samples were withdrawn at regular time intervals (1, 3, and 5 h), diluted and spread on freshly prepared Mueller Hinton agar plates. These plates were kept overnight in an incubator at 37 °C, and bacterial colonies were counted on next morning. Control experiments (*Staphylococcus aureus* + catalyst without light) were also performed. The bacterial inactivation efficiency of heterojunctions was calculated using eq 5.

$$\ln\left(\frac{N_t}{N_0}\right) = -kt \tag{5}$$

Where N_0 is the number of colony forming units (CFU) at 0 min, N_t is the number of CFUs after irradiation for t minutes, k is the inactivation rate constant, and N_t/N_0 is the survival ratio.[20] The survival ratio was calculated by normalizing the resultant CFUs on any plate to that on the plate without light exposure. Visible-light induced antibacterial experiments were triplicated, and the calculated *Stagphylococcus aureus* inactivation rate constants were within a 10% error limit.

dx.doi.org/10.1021/am302676a | ACS Appl. Mater. Interfaces 2013, 5, 1663−1672

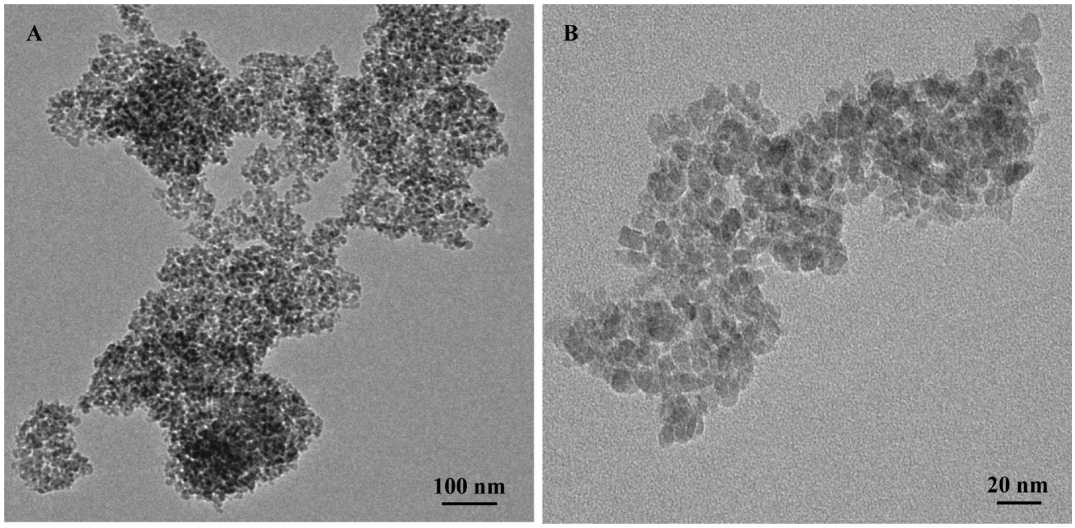

Figure 3. (A and B) Transmission electron micrograph of carbon-doped anatase-brookite heterojunctions prepared by 60 min microwave irradiation.

3. RESULTS AND DISCUSSION

3.1. Formation of Carbon-Doped Heterojunctions. The effect of microwave treatment on the amorphous to crystalline transition and crystallite size of titania was investigated using X-ray diffraction (XRD) studies. The absence of any characteristic peaks in the diffraction pattern of the precursor material before microwave treatment has confirmed its amorphous nature. Amorphous to crystalline transition and an increase of crystallite size was identified on microwave treatment (Figure 1A). For example, after 20 min of microwave irradiation, the XRD pattern consists of peaks corresponding to anatase and brookite phase titania with an average crystallite size of 7 ± 2 nm. Whereas 10 min irradiation was found to be not sufficient for the formation of crystalline titania. A crystallite growth was also observed with an increase of microwave irradiation time, and no significant increase of crystallite size was observed after 10 ± 2 nm, which was achieved after 40 min of microwave irradiation. Irrespective of the irradiation time, the crystalline titania contains 80% of anatase and 20% of brookite (peak at $2\theta = 31.16$).[15] The more surface sensitive Raman spectroscopic results were also in strong agreement with the phase composition obtained from XRD results (Figure 1B). Raman spectra of amorphous titania before microwave treatment were featureless, and bands observed at 147, 197, 396, 516, and 638 cm^{-1} for crystalline titania obtained after microwave treatment can be assigned to the presence of the major anatase phase.[3−5] Whereas the additional peaks at 247, 318, and 366 cm^{-1} are characteristic of the brookite phase.[21] The effect of heat treatment on amorphous and microwave treated nanocrystalline titania were investigated using differential scanning calorimetry (DSC). Both amorphous and microwave treated crystalline titania samples have endothermic peaks below 100 °C (Figure 2A), which represents the removal of water molecules and other volatile impurities.[3] The amorphous titania has an exothermic peaks characteristic of anatase phase crystallization at 403 °C. Meanwhile, the absence of such exothermic peaks for 20 min microwave treated titania confirmed its 100% crystallinity. These results demonstrate that 20 min non-hydrothermal microwave treatment of amorphous titania result in the formation of crystalline anatase-brookite nano-heterojunctions. The rapid crystallization observed can be attributed to the effective molecular level heating resulting from microwave irradiation.

The effect of microwave treatment on the structure of titanium tetraisopropoxide (TTIP), formation of crystalline titania, and nature of dopants were also identified from the FTIR analysis (Figure 2B). TTIP has peaks corresponding to Ti−O bonds at 620 cm^{-1}, and peaks at 2920, 1463, and 1005 cm^{-1} are characteristic of C−H stretching, scissoring, and bending modes, respectively.[22] Additional peaks at 1371 and 1141 cm^{-1} represent CH_3 deformation and C−O stretching of TTIP.[23] None of these peaks were present in the FTIR spectra of microwave treated crystalline titania, which proved the complete hydrolysis of TTIP and the phase purity of anatase-brookite heterojunctions. Formation of a Ti−O−Ti network in the microwave treated nanocrystalline titania was detected from the peak at 630 cm^{-1}. In addition, existence of carbon as carbonate ions was identified from its distinctive peak at 798 cm^{-1}.[24] A sharp peak at 1623 cm^{-1} and broad peaks at 3000−3600 cm^{-1} are characteristic of bending and stretching vibrations of the OH group of surface adsorbed water molecules.[5,25] Transmission electron microscopic images of the heterojunctions have demonstrated the uniform particle size distribution of carbon-doped anatase-brookite heterojunctions (Figure 3). In addition, the particle sizes of heterojunctions obtained from the transmission electron microscopy (TEM) analysis were consistent with the average particle sizes obtained from the XRD studies. For instance, the average particle size of 60 min microwave treated titania was 10 ± 2 nm, which was in good agreement with the average particle size obtained from XRD analysis. Nitrogen adsorption isotherms of carbon-doped anatase-brookite heterojunctions showed type IV characteristics with H1 type of hysteresis (Figure 4). Superior textural properties were observed for these titania samples prepared through nonhydrothermal microwave method. For example, the specific surface area and the pore volume of the C-doped heterojunctions were significantly higher than the standard commercial photocatalyst Evonik-Degussa P-25 (Table 1). As mentioned earlier, maintaining the mesoporosity and surface area during amorphous to crystalline transition is a major challenge in the synthesis of semiconductor photocatalysts. In the present case, nonhydrothermal microwave treatment results in the crystallization of nano-

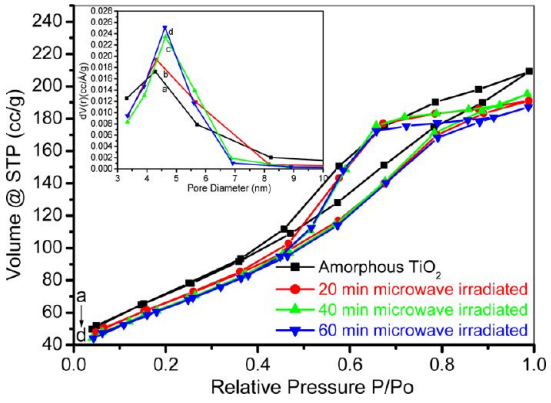

Figure 4. N_2 adsorption−desorption isotherm and the pore size distribution (inset) of (a) amorphous TiO_2, (b) 20 min microwave-irradiated TiO_2, (c) 40 min microwave-irradiated TiO_2, and (d) 60 min microwave-irradiated TiO_2.

Table 1. Textural Properties of Carbon-Doped Anatase-Brookite Heterojunctions (Error ±5%)

composition	surface area (m^2/g)	pore diameter (nm)	pore volume (cc/g)
amorphous	260	4.28	0.28
20 min microwave	242	4.32	0.28
40 min microwave	233	4.63	0.27
60 min microwave	231	4.61	0.27
Evonik-Degussa P-25	46	3.89	0.13

structured carbon-doped anatase-brookite heterojunctions without compromising textural properties. For instance, photocatalytically most active heterojunctions obtained after 60 min microwave treatment has a surface area and pore diameter of 231 m^2/g and 4.61 nm, respectively (Table 1).

Presence of carbon in the heterojunctions was identified from the X-ray photoelectron spectroscopy (XPS) results. In the deconvoluted C 1s high resolution XPS spectra (Figure 5A), the peak at 285 eV is characteristic of C—C, C═C, and C—H bonds (adventitious carbon).[3,4] Additional peaks at higher binding energies of 287.5, 289, and 291 eV can be assigned to C—O, C═O, and carbon bound to the three oxygen atoms in the carbonate ions.[10,26−28] C 1s peak characteristic of the Ti—C bond was absent in these XPS spectra, which rules out the carbon doping in the TiO_2 lattice. Independent of the microwave irradiation time, all the heterojunctions contain 6 at % of carbon impurities. The presence of carbonate ions in the anatase-brookite heterojunctions was in agreement with the FTIR peak at 798 cm^{-1}, and previous studies by Sakthivel et al.[10,24] The Ti/C and O/C ratios of heterojunctions determined from XPS results were 3.935 and 9.855, respectively, which are comparable to previous reports of carbon-doped titania.[29] Existence of carbon as carbonate ions were further confirmed by Raman spectral analysis (Figure 5B inset). Raman bands at 1064 and 1415 cm^{-1} are characteristic of carbonate ions present in the carbon-doped heterojunctions.[30] It was previously shown that metal oxide semiconductors such as TiO_2 and ZnO can photoreduce and decompose carbon materials.[6,8,9,31−34] In order to investigate the chemical stability of carbon-doped heterojunctions, XPS analysis was performed after 20 h of visible-light irradiation (Supporting Information Figure S3). No change in the chemical state of carbon impurities was observed for the visible-light irradiated samples, which demonstrate the superior chemical stability of carbon-doped titania heterojunctions.

Increased Ti 2p and O 1s binding energies of carbon-doped heterojunctions (Supporting Information Figure S4) in comparison to pure titania can be attributed to the formation of bidentate complexes between titanium cation and carbonate ions. It is previously reported that in the presence of water, extremely reactive titanium alkoxides hydrolyze and subsequently polymerize to form a three-dimensional amorphous oxide network.[16] The size, stability, and morphology of the amorphous titania particles obtained from alkoxide is strongly dependent on the H_2O:Ti molar ratio. The formation of colloidal TiO_2 at a high H_2O:Ti ratio is of great interest because of the small size of particles (<100 nm) formed under these conditions. These amorphous titania particles obtained can be converted to crystalline titania by proper heat treatment. In the present case, microwave treatment of amorphous titanium dioxide nanoparticles formed by the hydrolysis of TTIP with excess water (H_2O:Ti = 10:1) result in the formation of carbon-doped anatase-brookite nano-heterojunctions possessing superior textural properties.

3.2. Electronic Structure of Carbon-Doped Heterojunctions. Significant red-shift in the UV−vis absorption spectra was observed for carbon-doped anatase-brookite heterojunctions compared to pure anatase titania (Figure 5B).

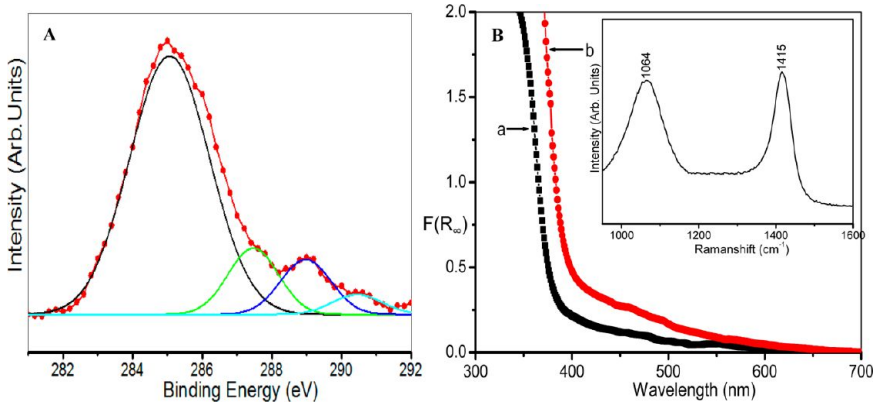

Figure 5. (A) C 1s XPS peaks and (B) optical absorption spectra of (a) anatase TiO_2 and (b) carbon-doped anatase-brookite heterojunctions prepared by 60 min microwave irradiation. (inset) Raman spectra demonstrating the presence of carbonate ions in carbon-doped anatase-brookite heterojunctions.

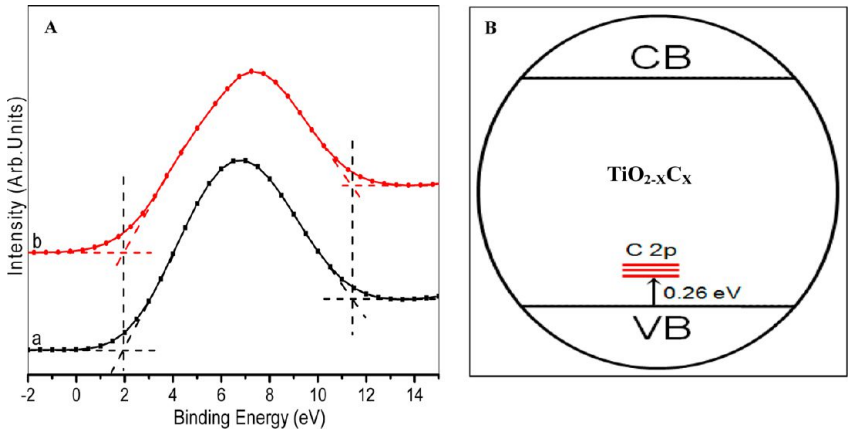

Figure 6. (A) Valence band XPS spectra of (a) anatase TiO_2 and (b) carbon-doped anatase-brookite heterojunctions prepared by 60 min of microwave irradiation. (B) Electronic structure of carbon-doped TiO_2.

The calculated band gap values of carbon-doped titania heterojunctions and pure anatase titania were 2.90 and 3.16 eV, respectively. Similar red-shift for carbon-doped TiO_2 had been also identified by previous researchers, and visible-light absorption was attributed to the presence of Ti^{3+} species and oxygen vacancies formed as a result of carbon doping.[10,11] On the basis of density state calculations, previous researchers also concluded that C-atom substitute for O^{2-} in the TiO_2 crystal structure, and the band gap narrowing results from the mixing of C 2p states with O 2p states (Ti−C bond).[35,36] It was also previously shown that chemical bonding between TiO_2 and carbon of graphene sheets can occurr in a TiO_2/graphene composite by formation of a chemical Ti−C bond.[6,37−40] In those works, formation of a Ti−C bond was distinguished as the important parameter in the photocatalytic performance. However, the local density approximation (LDA) calculations of anion-doped anatase TiO_2 conducted recently revealed that the band gaps of anion-doped TiO_2 are actually not narrowing and the observed visible-light absorption results from the isolated impurity states in the band gap.[41] These theoretical calculations also proved that lattice doping of anions is not necessary for band gap narrowing.

As identified from the XPS and FTIR studies, carbon-doped anatase-brookite heterojunctions contain carbonate ions. Valence band (VB) XPS was also performed in order to investigate the effect of carbonate impurities on the electronic structure of titania (Figure 6A). The VB maximum of 1.95 eV obtained for the undoped and carbon-doped anatase-brookite heterojunctions was identical to the previously reported VB-maximum level of pure anatase titania.[4,5,42] Moreover, the equal width of their VB of 9.5 eV represents almost similar mobilities of the photogenerated charge carriers. These results rule out the possibility of band gap narrowing due to mixing of C 2p bands with O 2p bands. The electronegativity of dopant atoms is an important factor that extensively determines the nature of doping.[3,5,41] As a result of the low electronegativity of carbon atoms in contrast to oxygen (3.44), only poor mixing of C 2p bands with O 2p bands can be expected for C-doped TiO_2.[41] In contrast, three 2 p bands of carbon atom still lie in the band gap of TiO_2, which can greatly reduce energy for the valence band to the conduction band electronic transition.[41] Therefore, the band gap narrowing for the carbon-doped anatase-brookite heterojunctions can be explained by the isolated C 2p states of carbonate ions in the band gap of TiO_2 rather than the C 2p and O 2p mixing theory. Since the band gap values of pure anatase and carbon-doped heterojunctions are 3.16 and 2.90 eV, respectively, the C 2p states should be 0.26 eV above the valence band of undoped titania (Figure 6B). It should be noted that XPS peaks characteristic of Ti−C bonds (281.9 eV) were absent in the C 1s XPS spectra of the C-doped heterojunctions, which rules out the replacement of O^{2-} ions of TiO_2 lattice carbon atoms.[35,36] Furthermore, slightly higher Ti 2p and O 1s binding energies of carbon-doped heterojunctions compared to pure anatase titania exclude the band gap narrowing related to Ti^{3+} ions and oxygen vacancies (Supporting Information Figure S4). Thus, it can be concluded that the additional energy levels created by carbonate ions are responsible for the band gap narrowing of the carbon-doped anatase-brookite heterojunctions.

3.3. Visible-Light Induced Photocatalytic and Antibacterial Study. Visible-light induced photocatalytic and antibacterial activities of carbon-doped anatase-brookite heterojunctions (80% anatase + 20% brookite) were significantly higher than the standard commercial photocatalyst Evonik-Degussa P-25 (70% anatase + 30% rutile). Among the different microwave-treated samples, photocatalytic activity increased with an increase of microwave irradiation time (Supporting Information Table S1), and there was no significant increase in the activity after 40 min of microwave irradiation. Very poor photocatalytic activity of the amorphous titania and an increase in the activity up on microwave treatment can be related to an increase in the crystallinity during microwave irradiation. The most active heterojunction obtained after 60 min microwave treatment exhibited 2-fold higher visible-light activity compared to the standard commercial photocatalyst Evonik-Degussa P-25 (Figure 7). The calculated rate constants for methylene blue degradation using Evonik-Degussa P-25 and carbon-doped heterojunctions were 0.004 and 0.008 min^{-1}, respectively. In addition, the increased blue shift of UV/vis spectra during the photocatalytic degradation of methylene blue with carbon-doped heterojunctions (Supporting Information Figure S5) can be correlated to the faster dye degradation through the N-demethylation mechanism.[3−5] Under similar experimental conditions, the photocatalytic rate constants of Kronos VLP 7000 titania and brookite titania (synthesized by thermolysis of $TiCl_4$) were 0.0028 and 0.0016 min^{-1}, respectively (Supporting Information Figure S6).

Superior photocatalytic activity of Evonik-Degussa P-25 in contrast to Kronos VLP 7000 and brookite titania can be attributed to the synergetic effect due to the presence of 70%

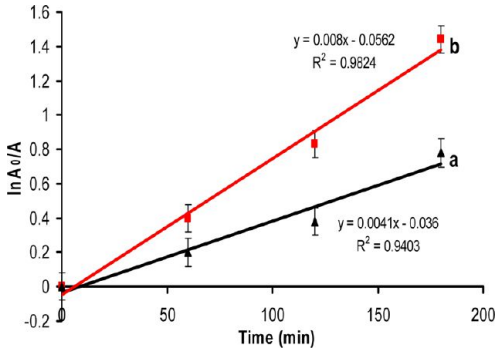

Figure 7. Photocatalytic kinetic study of visible-light induced methylene blue degradation using (a) Evonik-Degussa P-25 and (b) carbon-doped anatase-brookite heterojunctions prepared by 60 min microwave irradiation (error ±5%).

anatase and 30% rutile phases in P-25. In order to further confirm the photocatalytic activity of heterojunctions, methylene blue degradation experiments were also performed under visible-light generated by Q-Sun solar simulator and a primary green filter with a transmission intensity of 35% at 525 nm (Supporting Information Figure S7). In this case, Evonik-Degussa P-25 and the most active carbon-doped heterojunction exhibited photocatalytic rate constants of 0.001 and 0.007 cm^{-1}, respectively (Supporting Information Figure S8). Moreover, methylene blue solution containing heterojunctions appeared to be colorless after 5 h of continuous visible-light irradiation (Supporting Information Figure S9). The long-term photocatalytic activity of carbon-doped heterojunctions was investigated by repeating the methylene blue degradation experiments with the same photocatalyst. After 20 h of methylene blue degradation, carbon-doped heterojunctions exhibited 90% of the initial photocatalytic rate constant (Supporting Information Figure S10). These results clearly demonstrate the superior visible-light induced photocatalytic activities of carbon-doped anatase-brookite nano-heterojunctions.

In the absence of visible-light both Evonik-Degussa P-25 and the most active carbon-doped heterojunctions were inactive toward *Staphylococcus aureus* (Figure 8A and B). On the other hand, carbon-doped heterojunctions exhibited significantly higher visible-light induced antibacterial activity in contrast to the standard commercial photocatalyst Degussa P-25 (Figure 8C and D). The agar plates containing the standard photocatalyst were bacterial colony rich (116 colonies) after 5 h of visible-light radiation, whereas those containing the visible-light active carbon-doped heterojunctions contained only three bacterial colonies. This means that the survival ratio of bacterial colonies in the presence of $TiO_{2-x}C_x$ heterojunctions is much lower compared to that in presence of the standard photocatalyst (Figure 9). The photocatalytic inactivation rate constant for *Staphylococcus aureus* in the

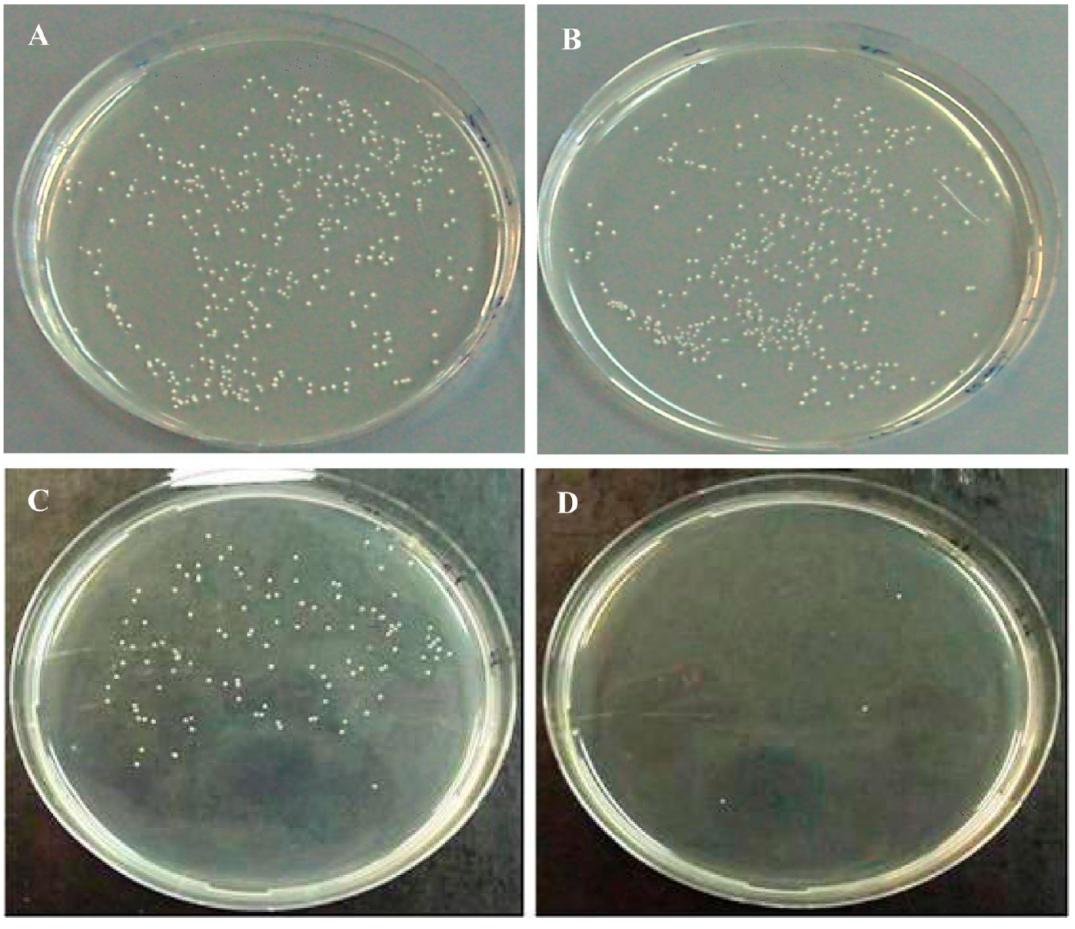

Figure 8. Bacterial colony growth in the presence of titania nanoparticles. (A) Evonik-Degussa P-25 without visible-light irradiation. (B) Carbon-doped anatase-brookite heterojunctions without visible-light irradiation. (C) Evonik-Degussa P-25 with visible light irradiation. (D) Carbon-doped anatase-brookite heterojunctions with visible-light irradiation.

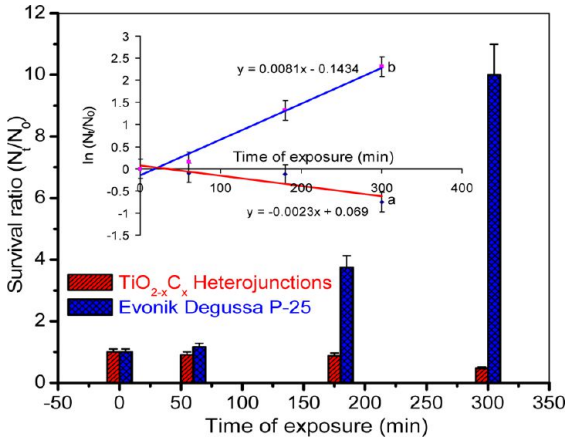

Figure 9. Survival ratios as a function of exposure duration for *Staphylococcus aureus* in the presence of carbon-doped anatase-brookite ($TiO_{2-x}C_x$) heterojunctions and Evonik Degussa P-25. (inset) Kinetic study of visible-light induced *Staphylococcus aureus* deactivation using (a) carbon-doped anatase-brookite heterojunctions and (b) Evonik-Degussa P-25 (error ±10%).

presence of carbon-doped nano-heterojunctions and Evonik-Degussa P-25 was 0.0023 and −0.0081 min^{-1}, respectively (Figure 9 inset). Mild antibacterial activity of Evonik-Degussa P-25 can be related to the visible-light absorption by 30% of a small band gap (3 eV) rutile phase. The inactivity of carbon-doped heterojunctions toward *Staphylococcus aureus* in the absence of visible-light confirmed the fact that photogenerated electron−hole pairs are responsible for the antibacterial activity.

The mechanism of UV-light induced bacterial killing using titanium dioxide has been well-documented.[43,44] The primary step involves the photoinduced generation of electron hole pairs. Electron in the conduction band can reduce O_2 to produce superoxide radicals ($\bullet O_2^-$). Further oxidation of $\bullet O_2^-$ by photogenerated holes results in the formation of singlet oxygen ($^1O_2$).[45] The hole in the valence band can also react with H_2O or OH^- adsorbed on the surface to produce hydroxyl radicals (•OH), hydrogen peroxide (H_2O_2), and protonated superoxide radical ($\bullet HO_2$). H_2O_2 in the valence band is reported to be resulting from the coupling of two •OH.[46] Further reaction of H_2O_2 with •OH forms protonated superoxide radical ($\bullet HO_2$) that functions like $\bullet O_2^-$ to inactivate the bacterial cells.[47] Thus •OH is suggested to play a crucial role in the production of H_2O_2 and $\bullet HO_2$ in the valence band. The photogenerated electron−hole pairs and the reactive oxygen species (ROS) resulting from their reaction with H_2O, OH^-, and O_2 results in the decomposition of bacteria.

It is reported that the photocatalytic killing mechanism initially damages the surface weak points of the bacterial cells, before total breakage of the cell membranes.[43] The internal bacterial components then leak from the cells through the damaged sites. Finally, the photocatalytic reaction oxidizes the cell debris. Complete oxidation of *Escherichia coli* cells to carbon dioxide using UV-light active titanium dioxide has been reported previously.[48] In the present case, when carbon-doped anatase-brookite heterojunctions are exposed to visible-light, electrons are promoted from the localized C 2p midgap level to the conduction band. Various ROS thus generated attacks and decompose the *Staphylococcus aureus* bacterial cells (Figure 10). Reduction of graphene oxide materials by bacteria (in the absence of TiO_2) have been recently reported by a number of researchers.[49] These reports point out a serious question regarding the stability of carbon impurities present in visible-light active titania during the antibacterial reaction. However in our opinion, electrons, holes, and other reactive oxygen species (ROS) produced by visible-light active TiO_2 result in the rapid decomposition of bacteria, making the bacterial reduction of carbon oxides almost impossible.

The superior visible-light induced photocatalytic and antibacterial activity of carbon-doped anatase-brookite heterojunctions can be explained on the basis of band gap narrowing, nanocrystalline nature of titania, improved textural properties, and coexistence of multiple phases. It is clear from the XRD, Raman, FTIR, XPS, and UV−vis spectroscopy results that the hydrolysis of titanium isopropoxide followed by nonhydrothermal microwave treatment result in the formation of carbon-doped anatase-brookite heterojunctions. In the present study, additional energy levels due to carbonate ions cause an effective band gap narrowing, which results in the superior visible-light induced photocatalytic and antibacterial activities. In addition,

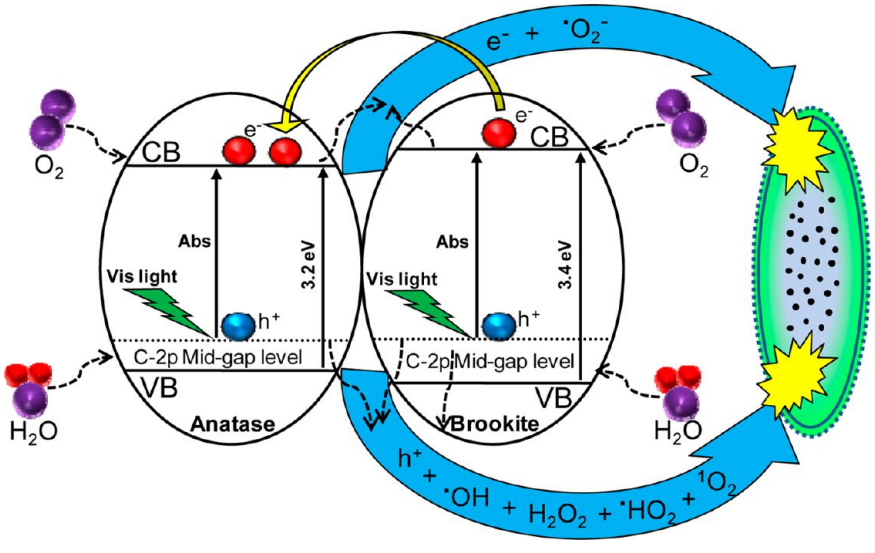

Figure 10. Mechanism of visible-light induced photocatalytic bacterial killing using carbon-doped anatase-brookite heterojunctions.

an increase in the surface acidity of TiO_2 due to the electron-withdraws inductive effect of carbonate ions on the Ti^{4+} ion also result in an enhancement of photocatalytic activity. Nanocrystalline nature of the heterojunctions may be another critical reason responsible for the improved visible-light induced photocatalytic activities. It is clear from the XRD and TEM results that the low temperature nonhydrothermal microwave method results in the formation of nanocrystalline titania without excessive particle growth. These anatase-brookite heterojunctions possess extremely higher surface area, increased pore diameter and superior pore volume compared to the Evonik-Degussa P-25 (Table 1). Consequently, these heterojunctions can adsorb and decompose methylene blue (MB) more efficiently. For example, the most active carbon-doped heterojunction with a surface area of 231 m^2/g adsorb more MB than the Evonik-Degussa P-25 with a surface area of 46 m^2/g (Supporting Information Figure S11). Increased surface area of the heterojunctions can also facilitate effective bacterial decomposition by increasing the contact between the catalyst nanoparticles and the bacteria. Thus, it can be concluded that the improved textural properties of anatase-brookite heterojunctions due to the nanocrystalline nature is a key factor responsible for their superior photocatalytic and antibacterial activities.

In order to investigate the effect of brookite phase on the efficiency of charge carrier trapping and their recombination single phase and heterojunction titania samples were subjected to photoluminescence (PL) spectroscopy. This technique has been employed previously to investigate the fate of photo-excited charge carriers and demonstrated a strong correlation between the PL intensity and the photocatalytic activity.[3−5] PL spectrum of pure anatase and brookite phase titania has characteristic band−band peaks at 386 and 378 nm, respectively (Figure 11). Band−band PL emission of

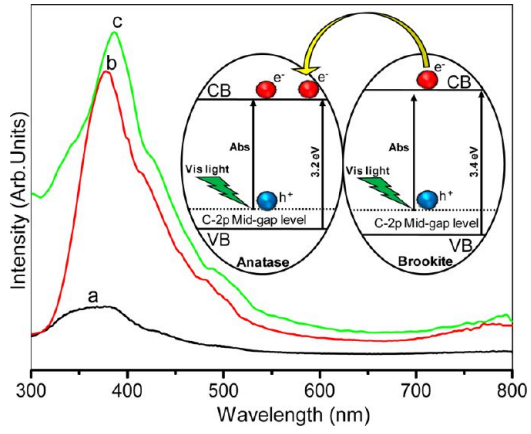

Figure 11. Photoluminescence spectra of (a) carbon-doped anatase-brookite heterojunctions prepared by 60 min microwave irradiation, (b) brookite TiO_2, (c) anatase TiO_2. (inset) Electron transfer mechanism in carbon-doped anatase-brookite heterojunctions.

heterojunctions were broad due to its nanocrystalline nature and mixed contribution from individual anatase/brookite phases. Additional low-intensity excitonic emission peaks appeared at higher wavelengths of 425 and 488 nm. Much higher band−band and excitonic PL intensities were identified for pure anatase and brookite titania in contrast the photocatalytically most active carbon-doped anatase-brookite heterojunctions. This demonstrates the fact that the coexistence of anatase and brookite phase is responsible for the decrease in PL intensities and superior photocatalytic activity of carbon-doped anatase-brookite heterojunctions.

Phase composition of titania is an important factor determining the PL intensities and photocatalytic activity of titania.[3−5,13,14] Photocatalysis involves the formation of electron−hole pairs through the photoexcitation of valence band electrons and their competitive recombination. Any factor reducing the electron−hole recombination rate results in a decrease of the PL intensity and an increase of the photocatalytic activity. Superior photocatalytic activities of titania heterojunctions related to their lower PL intensities have been reported previously.[3,5] As discussed previously, photocatalytically most active carbon-doped heterojunctions contained 80% anatase and 20% brookite, both possessing an average particle size of 10 ± 2 nm. Since the conduction band of brookite phase is ∼0.2 eV higher than that of the anatase titania, highly mobile photoexcited electrons (from the mid gap C 2p level) would rapidly transfer from the conduction band of brookite to that of anatase and leave the holes behind (Figure 11 inset).[50] This electron−hole separation stabilizes the photogenerated electron−hole pairs and slows down the charge carrier recombination, which results in an increase of visible-light induced photocatalytic and antibacterial activity. Additionally, photoexcited electrons formed on brookite can be transferred to the defect states of the anatase phase. It is therefore proposed that the efficient electron−hole separation due to brookite to anatase electron transfer is responsible for the superior visible-light induced photocatalytic and antibacterial activities of carbon-doped anatase-brookite heterojunctions.

4. CONCLUSIONS

Carbon-doped anatase-brookite nano-heterojunctions were synthesized for the first time through a nonhydrothermal microwave method. XRD and Raman spectroscopic techniques demonstrated revealed the fact that a low power microwave (300 W) irradiation for 20 min was enough for the amorphous to crystalline transition of titania. The presence of carbon as carbonate ions was identified from the FTIR and XPS results of heterojunctions. The electronic structure analysis using UV−vis and valence-band XPS revealed the fact that the formation of interband C 2p states was responsible for the band gap narrowing. The visible-light induced photocatalytic activity of the most active heterojunction was 2-fold higher in comparison to the standard commercial photocatalyst Evonik-Degussa P-25. Carbon-doped heterojunctions and Evonik Degussa P-25 exhibited *Staphylococcus aureus* inactivation rate constants of 0.0023 and −0.0081 min^{-1}, respectively. It has been proposed that the efficient electron−hole separation at the anatase-brookite interface is responsible for superior visible-light-induced photocatalytic and antibacterial activity of carbon-doped anatase-brookite nano-heterojunctions. The studies described herein demonstrate that carbon-doped anatase-brookite nano-heterojunctions can be effectively utilized for visible-light induced antibacterial applications.

■ ASSOCIATED CONTENT

Supporting Information

Transmission spectrum of primary blue filter. Absorption spectra of methylene blue at regular time intervals of visible-light irradiation in the absence of TiO_2. C 1s XPS pattern of carbon-doped heterojunctions after 20 h visible-light irradiation. Ti 2p and O 1s XPS pattern of carbon-doped

heterojunctions. Absorption spectra of visible-light induced methylene blue degradation. Photocatalytic kinetic study of Kronos VLP 7000 TiO_2 and brookite TiO_2. Transmission spectrum of primary green filter. Photocatalytic kinetic study of Evonik-Degussa P-25 and carbon-doped TiO_2 heterojunctions. Photographs of methylene blue solution containing carbon-doped heterojunctions before and after visible-light irradiation. Long-term photocatalytic activity of carbon-doped heterojunctions. Absorption spectra of methylene blue solution containing Evonik-Degussa P-25 and carbon-doped TiO_2 heterojunctions at regular time intervals in the absence of visible-light. Photocatalytic rate constants for visible-light induced methylene blue degradation using carbon-doped anatase-brookite heterojunctions. This information is available free of charge via the Internet at http://pubs.acs.org/

AUTHOR INFORMATION

Corresponding Author

*E-mail address: suresh.pillai@dit.ie.

Notes

The authors declare no competing financial interest.

ACKNOWLEDGMENTS

The authors would like to thank Enterprise Ireland for funding (CFTD/06/IT/326 and ARE/2008/0005). The authors would also like to thank Dr. John Colreavy for providing valuable comments.

REFERENCES

(1) Neu, H. C. *Science* **1992**, *257*, 1064−1073.
(2) Pelaez, M.; Nolan, N. T.; Pillai, S. C.; Seery, M. K.; Falaras, P.; Kontos, A. G.; Dunlop, P. S. M.; Hamilton, J. W. J.; Byrne, J. A.; O'Shea, K.; Entezari, M. H.; Dionysiou, D. D. *Appl. Catal., B* **2012**, *125*, 331−349.
(3) Etacheri, V.; Seery, M. K.; Hinder, S. J.; Pillai, S. C. *Chem. Mater.* **2010**, *22*, 3843−3853.
(4) Etacheri, V.; Seery, M. K.; Hinder, S. J.; Pillai, S. C. *Adv. Funct. Mater.* **2011**, *21*, 3744−3752.
(5) Etacheri, V.; Seery, M. K.; Hinder, S. J.; Pillai, S. C. *Inorg. Chem.* **2012**, *51*, 7164−7173.
(6) Akhavan, O.; Ghaderi, E. *J. Phys. Chem. C* **2009**, *113*, 20214−20220.
(7) Akhavan, O.; Ghaderi, E.; Rahimi, K. *J. Mater. Chem.* **2012**, *22*, 23260−23266.
(8) Akhavan, O.; Abdolahad, M.; Esfandiar, A.; Mohatashamifar, M. *J. Phys. Chem. C* **2010**, *114*, 12955−12959.
(9) Williams, G.; Seger, B.; Kamat, P. V. *ACS Nano* **2008**, *2*, 1487−1491.
(10) Sakthivel, S.; Kisch, H. *Angew. Chem., Int. Ed.* **2003**, *42*, 4908−4911.
(11) Asahi, R.; Morikawa, T.; Ohwaki, T.; Aoki, K.; Taga, Y. *Science* **2001**, *293*, 269−271.
(12) Umebayashi, T.; Yamaki, T.; Itoh, H.; Asai, K. *Appl. Phys. Lett.* **2002**, *81*, 454−456.
(13) Kavan, L.; Grtzel, M.; Gilbert, S. E.; Klemenz, C.; Scheel, H. J. *J. Am. Chem. Soc.* **1996**, *118*, 6716−6723.
(14) Kawahara, T.; Konishi, Y.; Tada, H.; Tohge, N.; Nishii, J.; Ito, S. *Angew. Chem., Int. Ed.* **2002**, *41*, 2811−2813.
(15) Boppella, R.; Basak, P.; Manorama, S. V. *ACS Appl. Mater. Interfaces* **2012**, *4*, 1239−1246.
(16) Pillai, S. C.; Periyat, P.; George, R.; McCormack, D. E.; Seery, M. K.; Hayden, H.; Colreavy, J.; Corr, D.; Hinder, S. J. *J. Phys. Chem. C* **2007**, *111*, 1605−1611.
(17) Komarneni, S.; Roy, R.; Li, Q. H. *Mater. Res. Bull.* **1992**, *27*, 1393−1405.
(18) Polshettiwar, V.; Varma, R. S. In *Aqueous Microwave Assisted Chemistry: Synthesis and Catalysis*, 1st ed.; Royal Society of Chemistry: London, 2010, pp 186−209.
(19) Nadagouda, M. N.; Varma, R. S. *Smart Mater. Struct.* **2006**, *15*, 1260−1265.
(20) Pal, A.; Pehkonen, S. O.; Yu, L. E.; Ray, M. B. *J. Photochem. Photobiol., A* **2007**, *186*, 335−341.
(21) Tian, G.; Fu, H.; Jing, L.; Xin, B.; Pan, K. *J. Phys. Chem. C* **2008**, *112*, 3083−3089.
(22) Hafizah, N.; Sopyan, L. *Int. J. Photoenergy* **2009**, *2009*, 1−8.
(23) Urlaub, R.; Posset, U.; Thull, R. *J. Non-Cryst. Solids* **2000**, *265*, 276−284.
(24) Gablenz, S.; Abicht, H. P.; Pippel, E.; Lichtenberger, O.; Woltersdorf, J. *J. Eur. Ceram. Soc.* **2000**, *20*, 1053−1060.
(25) Etacheri, V.; Roshan, R.; Kumar, V. *ACS Appl. Mater. Interfaces* **2012**, *4*, 2717−2725.
(26) Etacheri, V.; Haik, O.; Goffer, Y.; Roberts, G. A.; Stefan, I. C.; Fasching, R.; Aurbach, D. *Langmuir* **2012**, *28*, 965−976.
(27) Etacheri, V.; Geiger, U.; Gofer, Y.; Roberts, G. A.; Stefan, I. C.; Fasching, R.; Aurbach, D. *Langmuir* **2012**, *28*, 6175−6184.
(28) Akhavan, O.; Ghaderi, E.; Akhavan, A. *Biomaterials* **2012**, *33*, 8017−8025.
(29) Yu, J.; Dai, G.; Xiang, Q.; Jaroniec, M. *J. Mater. Chem.* **2011**, *21*, 1049−1057.
(30) Scheetz, E. B.; White, B. W. *Am. Mineral.* **1977**, *62*, 36−50.
(31) Akhavan, O. *ACS Nano* **2010**, *4*, 4174−4180.
(32) Williams, G.; Kamat, P. V. *Langmuir* **2009**, *25*, 13869−13873.
(33) Akhavan, O. *Carbon* **2011**, *49*, 11−18.
(34) Akhavan, O.; Choobtashani, M.; Ghaderi, E. *J. Phys. Chem. C* **2012**, *116*, 9653−9659.
(35) Irie, H.; Watanabe, Y.; Hashimoto, K. *Chem. Lett.* **2003**, *32*, 772−773.
(36) Khan, S. U. M.; Al-Shahry, M.; Ingler, W. B. *Science* **2002**, *297*, 2243−2245.
(37) Chena, L. C.; Hoa, Y. C.; Guoa, W. S.; Huangb, C. M.; Pan, T. C. *Electrochim. Acta* **2009**, *54*, 3884−3891.
(38) Akhavan, O.; Abdolahad, M.; Abdib, Y.; Mohajerzadeh, S. *Carbon* **2009**, *47*, 3280−3287.
(39) Yu, H.; Quan, X.; Chen, S.; Zhao, H.; Zhang, Y. *J. Photochem. Photobiol., A* **2008**, *200*, 301−306.
(40) Akhavan, O.; Azimirad, R.; Safa, S.; Larijani, M. M. *J. Mater. Chem.* **2010**, *20*, 7386−7392.
(41) Segall, M. D.; Lindan, P. J. D.; Probert, M. J.; Pickard, C. J.; Hasnip, P. J.; Clark, S. J.; Payne, M. C. *J. Phys.: Condens. Matter* **2002**, *14*, 2717−2744.
(42) Pan, J.; Liu, G.; Lu, G. Q.; Cheng, H. M. *Angew. Chem., Int. Ed.* **2011**, *50*, 2133−2137.
(43) Rengifo-Herrera, J. A.; Pulgarin, C. *Sol. Energy* **2010**, *84*, 37−43.
(44) Byrne, J. A.; Fernandez-Ibanez, P. A.; Dunlop, P. S. M.; Alrousan, D. M. A.; Hamilton, J. W. J. *Int. J. Photoenergy* **2011**, *2011*, 1−12.
(45) Daimon, T.; Hirakawa, T.; Kitazawa, M.; Suetake, J.; Nosaka, Y. *Appl. Catal., A* **2008**, *340*, 169−175.
(46) Sakai, H.; Baba, R.; Hashimoto, K.; Fujishima, A. *J. Phys. Chem.* **1995**, *99*, 11896−11900.
(47) Harbour, J. R.; Hair, M. L. *J. Phys. Chem.* **1979**, *83*, 652−656.
(48) Jacoby, W. A.; Maness, P. C.; Wolfrum, E. J.; Blake, D. M.; Fennel, J. A. *Environ. Sci. Technol.* **1998**, *32*, 2650−2653.
(49) Akhavan, O.; Ghaderi, E. *Carbon* **2012**, *50*, 1853−1860.
(50) Zhao, B.; Chen, F.; Jiao, Y.; Yang, H.; Zhang, J. *J. Mol. Catal. A: Chem.* **2011**, *348*, 114−119.